intracranial electrodes). Written informed consent was obtained from all patients and their families.

Electrodes

We designed microwireelectrodes for single-unit/LFP recording combined with a polyamide depth electrode for iEEG recording (Unique Medical, Tokyo, Japan) (Fig. 1). While the basic concept of the electrodes draws on Behnke-Fried electrodes,[11]the main difference here was the design of a depth-iEEG electrode. We made it of polyamide, which is stiffer and less flexible than silicon. The electrode-microwirelead complex was L-shaped as a whole. Thus, handling it in the craniotomy field was easier and the positional stability after implantation was better. We fabricated the inner stylet to be attached firmly to the pointer probe of the navigation system (Fig. 1). We put a silicon fringe at the end of the electrode to prevent subduction into the brain in patients later in the series (Fig. 1C). The depth-iEEG electrode has two or six 2-mm-wide platinum contacts with inter-contact separations of 2 mm.The lengths of the depth electrodes were preoperatively determined according to the planned trajectory in 3-D T1-weighted MRIs of the subject's brain, which consisted of 136 sequential 1.4-mm-thick axial slices with a resolution of 256 x 256 pixels in a field of view of 240mm, using medical imaging software (OsiriX).For each hippocampus, we planned two depth electrodes whose tips were located in the lateral area of the subiculum in the head and body of the hippocampus. The entry point and trajectory were determined to avoid passing through the sulci. In most cases, the entry point was at the middle temporal gyrus, but in some cases it was at the superior or inferior temporal gyrus. We avoided passing through the ventricle in principle, but could not in some cases, particularly when the entry point was at the superior temporal gyrus. We chose a non-orthogonal trajectory that was as vertical as possible to the brain surface.

In addition, eightmicrowires made of 80-ìm platinum/iridium were inserted through the lumen, extending 1.5 to 5 mm beyond the tip of the depth electrode to record neuronal activity from various layers of the hippocampus or subiculum. The impedance of each microwire was in the range of 300 to 500 kÙ. We fixed the end of the microwires and depth electrodes with an instant adhesive immediately after insertion of the former into the latter, so that the whole electrode-microwirelead complexwould pulsate with the brain, with the expectation of potential long-term micro-recording stability.

For surface iEEG, we used grid, strip and trapezoidelectrodes (Unique Medical, Tokyo, Japan) with either 3-mm-diameter platinum contactsand a 10-mm separation or 1.5-mm-diameter contacts with a 5-mm separation. The number and location of the recording sites were determined solely based on clinical factors.

Surgical procedures

Under general anesthesia, the patients' headswere fixed with a Mayfield radiolucent skull clamp. 3-D-fast spoiled gradient echo (SPGR) MRIs of the subject's brain, which consisted of 1.5-mm-thick axial slices with a resolution of 256 x 256 pixels in a field of view of 240mm, was integrated into a frameless navigation system (Signa HDxt 3.0Tesla; GE Healthcare, Milwaukee,WI,USA). Then the three-dimensional spatial coordinate was registered using superficial markers and a surface mergefor a navigation system (Stealth Station S7 Navigation; Medtronic Inc, MN, USA). Following craniotomy and dural opening, subdural grid/strip electrodes for surface iEEG were temporarily placed on the surface of the brain. We intraoperatively readjusted the entry point and trajectory of the depth electrodes according to the sulcal pattern so as to spare the cortical vessels and surrounding tissues. The placements of the surface grids were adjusted as well, and holes for depth-electrode insertion were made in the grids if necessary. The depth electrode was then placed. It was advanced to the target point manually under the guidance of a navigation system. The inner stylet was removed from the depth electrode. Then, strip and trapezoid electrodes for the ventral temporal surface and parahippocampal gyrus were placed under fluoroscopy.[19]We always put the parahippocampal surface electrode under fluoroscopy so that its most anterior contact is located just posterior to the sella turcica. We believe this method enables the consistent placement of the electrode in all patients.Because this step caused a significant loss in cerebrospinal fluid (CSF), we always placed the depth electrodes before placing the ventral strip/trapezoid electrodes. After all iEEG electrodes had been placed and fixed (Fig. 1D), we gently introduced the microwires through the lumen of the depth electrode using a preset thin insertion cannula (Fig. 1C). The depth electrode and the microwires were firmly glued together with medical-grade cyano acrylate(Aron alpha A, Toa-Gosei, Tokyo, Japan)immediately after the insertion. After all the procedures had beencompleted, the dura was tightly sutured and sealed with fibrin glue to prevent CSF leakage.

Electrode localization

All patients underwent high-resolution 3 Tesla T1-weighted volumetric MRI scans prior to electrode implantation, and high-resolution 0.5-mm-slice computerized tomography (CT) scans 3 to 9 days (mean 5.3 days) after surgery (Fig. 2A). MRI and CT images were then co-registered using 3-D constructing software (Dr.View; Asahi-kasei, Tokyo, Japan) (Fig. 2B). The locations of the microwires were inferred from their relative positions to the depth electrodes.

Recording and Data analysis

Continuous video-EEG monitoring was performed from post-operative Days 1 to 25 until a sufficient number of habitual seizures were recorded.The signals recorded from the microwireswere referenced to an electrode placed againstthe internal surface of the dura or in

the intracranial space outside of the epileptic focus. The signalswere analog-filtered between 0.3 and 7.5 kHz and sampled at 30 kHz(Cerebus; Blackrock Microsystems, UT, USA). For single-unit recording, the sampled data was digitally high-passfiltered at 750 Hz, and the local waveforms for whichthe negative peak fell below the 3.7 SD of the background signal were sorted offline using the T-distribution expectation-maximization paradigm (Offline sorter; PlexonInc, TX, USA). For LFP recording, the original data sampled at 30 kHz was down-sampled at 2 kHz. iEEG was referenced to an electrode placed on the scalp or against theinternal surface of the dura, filtered between 0.55 and 150 Hz and sampled at 400 Hz (NicoletOne, Care Fusion, CA, USA). The in-house Matlab (MathWorks, Natick, MA, USA) programs, with statistical toolbox, signal processing toolbox, and the open source Matlab toolbox EEGLABwere utilized for data analysis.[20]

Evaluation of the procedures

To assess the feasibility of our procedures, we examined the data in four ways. First, wecalculated the spatial error of our frameless-navigated implantation surgery. Three-dimensional coordinates of the target point, which was retrieved from the stored data of the navigation system, and the implanted point, which was determined from the overlay image of postoperative 3-D-CT, were measured; the gaps were calculated and then plotted on a 2- or 3-D display(Figs.2C, 3).Second, we evaluatedthetemporal stability of single-unit recording. The recording yield of the microelectrode was divided and analyzed every 5 days and then tested for significant differences among each recording period with the Kruskal-Wallis test. Third, we confirmed whether simultaneoussingle-unit, LFP and iEEG recording were successfully performed or not. The sorted single-unit data were transformed into a firing rate for a period of approximately 65 min and displayed as a histogram. iEEG data was Fourier-transformed for the correspondingperiod, which was worth 131,072 samples. These data and the raw LFP signal were displayed and compared in the same time series. Fourth, we recorded visually evoked responses and confirmed whether our methodology was applicable for cognitive study or not. The patients performed a familiar face detection task while gray-scaled photographs of 36 different faces, including four familiar faces of the patients' sister, father, mother and grandmother, were presented in random order on a PC monitor at a viewing distance of 100 cm. Each stimulus was presented for 1000 milliseconds (ms), followed by a 3000 ms interval period,using a Stimuli Output Sequencer (NoruPro Light Systems Inc., Tokyo, Japan).

Results

Post-operative CT revealed that depth-microwire electrodes implanted with a frameless navigation system were placed within a margin of error of 3.6 ± 2.3 mm (mean ± SD) (Figs. 2, 3). No surgical complications (e.g.,intracranial bleeding, CSF leakage,infection) were noted in anypatients in this series. We recorded single-unit activity, LFP and iEEG from 9

subjects in a chronic and/or subacute phase. One subject was excluded from recording rate and temporal stabilityanalysis because of damage to the ground/reference wire. The rates of successful recording of single- or multiple-unit activity with microwires ranged from 0 to 40.6% (mean: 14.8%)(Table 1). In the evaluation of recording stability, no significant differences were observed in the recording rate among each recording period (P=0.65; Kruskal-Wallis test) (Fig. 4). Finally, we compared the interictal-ictal neural activity recorded with a singleunit, LFP and iEEG in a local brain region of one patient(Fig. 5). In this epileptic seizure, firing rate and LFP, recorded from the microwire, and spectral power showed increasing activity prior to the clinical seizure onset. The earliest change was observed inLFP (Fig. 5, second row),followed by an increase in firing rate. We observed a trough in both firing rate and LFP immediately after the first local peak.

We also recorded a visually evoked single-unit response in some of the patients. Figure 6 shows a representative response recorded from the microwire in the hippocampus of Subject 2. This neuronal activitywas in response to the photograph of a particular family member, but not to those of the other members. The latency of the peak response was 400 ms, and the firing rate at the peak exceeded the mean + 2 SD of the rate in the pre-stimulus period.

Discussion

Single-unit recording hasa high temporal resolution of up to 30kHz, allowing us to evaluateunitary output events of neuronal activity.Although the studies using single-unit recording were applied to the very restricted regions of the brain, ithas provided fundamental and important information on the mechanism of human brain function.[21-25] By contrast, iEEG can cover a broad area of the cortical surface,allowing us tolocalize the functional and diseased area,as well as to clarify the association of multiple areas and the spread pattern of the disease.[26,27]To elucidate the relationship between the single-unit and ensemble activity of neuronsis crucial but has not been examined in humans because of technical difficulties.

In the present study, we fabricated a depth-microwire electrode for use with aframeless navigation system, which enabled the simultaneous placement of broad-area subdural electrodes. While the well-known Behnke-Fried electrodeshave already been commercially available in the United States, they were designed to be implantedwith a stereotactic frame and to be fixed to the skull. A frameless navigation system enabled us to implant depth-microwire electrodes at desired positions in a surgical setup without a stereotactic frame.We made our depth electrode shorter and stiffer for more precise implantation without bending of the shaft. We made the depth-microwire lead complex L-shaped so as to enable it to sit under the dura without protruding from the brain surface, with the expectation of easier handling in the craniotomy field and a natural pulsation with the brain. The expectations were achieved in two aspects. First, there was no complication associated with depth-electrode placement. Second, recording stability was maintained for longer than 3 weeks. Thislong-term stability

provided us enough time to record a sufficient number of habitual seizures and for the subjects to perform cognitive tasks. Some hippocampal neurons showed a preference for a particular member of the family. These characteristics matched the property of previously reported human hippocampal neurons.[28,27]

In terms of the implantation procedure, we paid special attention to the following three points: First, the trajectory of the depth electrodeswas determined to completely avoid the sulci and to be as vertical as possible to the brain surface in order to make the length of the electrode shorter and to decrease placement error. Second, we made an effort to minimize CSF loss and, thereby,the subsequent brain shift that affectsthe spatial accuracy of the depth-electrode implantation. We always placed the temporobasal electrodes after placing the depth electrodes, since placement of the former causes significant CSF loss.While the opening of the dura and placement of the surface grid before the depth electrodes did not cause significant CSF loss as long as they were performed smoothly and promptly, we adjusted the tilt of the bed and paid attention to the cotton used in the surgical field, ensuring that it did not cause a siphon effect. Third, it was important to determine the final entry point and implant the depth electrodes after placing the grid electrodes on the lateral temporal surface. We were afraid that placement of the depth electrodes in the first step of the procedure would increase the risk of extra injurious force to the brain and insufficient placement of surface grid electrodes.

In comparison with a frame-based stereotactic procedure, the spatial error of 3.6 mm waslarger. At the start of the present study, our objective was to place the tip of the microwires in the neuronal layers, and we had assumed that adepth-tip spatial error of up to 5 mm was acceptable because we could not control how the microwires would protrude and spread from the tip of the depth electrode. Therefore, we did not employ the Point Setter arm, which may have allowed forthe more steady advancement of the depth electrode and a smaller spatial error.[16] However, since the error was distributed almost equally in all directions, we attributed it mainly to the manual advancement of the depth electrode. If the error had been caused by brain shift, it would most likely have deviated in one direction. The employment of the arm may be efficient, particularly when the target is set in a specifically restricted region within the hippocampus. We are preparing such a system and will verify whether it improves spatial accuracy and the rate of successful micro recording.

Other factors that influence the micro-recording rate may include the learning curves of the implantation procedure and recording procedure, particularly regarding noise reduction techniques,microelectrode properties, and the nature of the target neuronal areas. We found a tendency in patients later in the series; namely, they showed higher recording rates and spatial accuracy even though we were using the same electrodes. Our microelectrodes had a larger diameter and a tapered tip with higher impedance than a Behnke-Fried electrode. An appropriate diameter and impedance must be determined in the future. Micro-recording from

the primary motor cortex using the Neuroport system renders a higher recording rate.[29]Since itintegrates an amplifierinto the electrode, providing a higher signal-to-noise ratio, we must clarify whether the employment of the technology improves the recording rate. We must clarify,as well,how differences in neuronal density, and distance from the surface, affect the recording rate.

Although increasing the type and number of electrodes may theoretically lead to a possible increase in complications, such as intracranial bleeding or infection, we did not experience such complications in the present series.However, we were able to confirm the safety of this techniquein a larger number of patients. Furthermore, recording stability for a much longer period than one month may be required in the future for use in epilepsy treatment and brain-machine interfaces. The presently available electrodes, including ours, are not sufficient for that purpose.[30]The effort to develop next generation electrodes must be continued.

References

1. Engel AK, Moll CK, Fried I, Ojemann GA. Invasive recordings from the human brain: clinical insights and beyond. *Nat Rev Neurosci*. 2005;6(1):35-47.
2. Keene DL, Whiting S, Ventureyra EC. Electrocorticography. *Epileptic Disord*. 2000;2(1):57-63.
3. Lai Y, van Drongelen W, Hecox K, et al. Cortical activation mapping of epileptiform activity derived from interictal ECoG spikes. *Epilepsia*. 2007;48(2):305-314.
4. Luther N, Rubens E, Sethi N, et al. The value of intraoperative electrocorticography in surgical decision making for temporal lobe epilepsy with normal MRI. *Epilepsia*. 2011;52(5):941-948.
5. Bower MR, Buckmaster PS. Changes in granule cell firing rates precede locally recorded spontaneous seizures by minutes in an animal model of temporal lobe epilepsy. *J Neurophysiol*. 2008;99(5):2431-2442.
6. Jiruska P, Csicsvari J, Powell AD, et al. High-frequency network activity, global increase in neuronal activity, and synchrony expansion precede epileptic seizures in vitro. *J Neurosci*. 2010;30(16):5690-5701.
7. Truccolo W, Donoghue JA, Hochberg LR, et al. Single-neuron dynamics in human focal epilepsy. *Nat Neurosci*. 2011;14(5):635-641.
8. Buzsaki G, Anastassiou CA, Koch C. The origin of extracellular fields and currents--EEG, ECoG, LFP and spikes. *Nat Rev Neurosci*. 2012;13(6):407-420.
9. Toda H, Suzuki T, Sawahata H, et al. Simultaneous recording of ECoG and intracortical neuronal activity using a flexible multichannel electrode-mesh in visual cortex. *Neuroimage*. 2010;54(1):203-212.

10. Radman T, Su Y, An JH, Parra LC, Bikson M. Spike timing amplifies the effect of electric fields on neurons: implications for endogenous field effects. *J Neurosci*. 2007;27(11):3030-3036.
11. Fried I, MacDonald KA, Wilson CL. Single neuron activity in human hippocampus and amygdala during recognition of faces and objects. *Neuron*. 1997;18(5):753-765.
12. Howard MA, Volkov IO, Noh MD, et al. Chronic microelectrode investigations of normal human brain physiology using a hybrid depth electrode. *Stereotactic and Functional Neurosurgery*. 1997;68(1-4):236-242.
13. Kratimenos GP, Thomas DG, Shorvon SD, Fish DR. Stereotactic insertion of intracerebral electrodes in the investigation of epilepsy. *Br J Neurosurg*. 1993;7(1):45-52.
14. Ulbert I, Halgren E, Heit G, Karmos G. Multiple microelectrode-recording system for human intracortical applications. *J Neurosci Methods*. 2001;106(1):69-79.
15. Spencer SS, Spencer DD, Williamson PD, Mattson R. Combined depth and subdural electrode investigation in uncontrolled epilepsy. *Neurology*. 1990;40(1):74-79.
16. Mehta AD, Labar D, Dean A, et al. Frameless stereotactic placement of depth electrodes in epilepsy surgery. *J Neurosurg*. 2005;102(6):1040-1045.
17. Murphy MA, O'Brien TJ, Cook MJ. Insertion of depth electrodes with or without subdural grids using frameless stereotactic guidance systems--technique and outcome. *Br J Neurosurg*. 2002;16(2):119-125.
18. Wray CD, Kraemer DL, Yang T, et al. Freehand placement of depth electrodes using electromagnetic frameless stereotactic guidance. *J Neurosurg Pediatr*. 2011;8(5):464-467.
19. Koizumi S, Kawai K, Asano S, et al. Familial lateral temporal lobe epilepsy confirmed with intracranial electroencephalography and successfully treated by surgery. *Neurol Med Chir (Tokyo)*. 2011;51(8):604-610.
20. Delorme A, Makeig S. EEGLAB: an open source toolbox for analysis of single-trial EEG dynamics including independent component analysis. *J Neurosci Methods*. 2004;134(1):9-21.
21. Azhar F, Anderson WS. Predicting single-neuron activity in locally connected networks. *Neural Comput*. 2012;24(10):2655-2677.
22. Howard MW, Viskontas IV, Shankar KH, Fried I. Ensembles of human MTL neurons "jump back in time" in response to a repeated stimulus. *Hippocampus*. 2012;22(9):1833-1847.
23. Jobst BC. What is a seizure? Insights from human single-neuron recordings. *Epilepsy Curr*. 2012;12(4):135-137.
24. Sheth SA, Mian MK, Patel SR, et al. Human dorsal anterior cingulate cortex neurons mediate ongoing behavioural adaptation. *Nature*. 2012;488(7410):218-221.

25. Suthana N, Fried I. Percepts to recollections: insights from single neuron recordings in the human brain. *Trends Cogn Sci*. 2012;16(8):427-436.
26. Wilke C, Ding L, He B. Estimation of Time-Varying Connectivity Patterns Through the Use of an Adaptive Directed Transfer Function. *Ieee Transactions on Biomedical Engineering*. 2008;55(11):2557-2564.
27. Zhang H, Benz HL, Bezerianos A, et al. Connectivity mapping of the human ECoG during a motor task with a time-varying dynamic Bayesian network. *Conf Proc IEEE Eng Med Biol Soc*. 2010:130-133.
28. Quiroga RQ, Reddy L, Kreiman G, Koch C, Fried I. Invariant visual representation by single neurons in the human brain. *Nature*. 2005;435(7045):1102-1107.
29. Patterson WR, Song YK, Bull CW, et al. A microelectrode/microelectronic hybrid device for brain implantable neuroprosthesis applications. *IEEE Trans Biomed Eng*. 2004;51(10):1845-1853.
30. Polikov VS, Tresco PA, Reichert WM. Response of brain tissue to chronically implanted neural electrodes. *J Neurosci Methods*. 2005;148(1):1-18.

Figure legends

Figure 1. A microwire-combined depth electrode. (A) Electrodedesign. The upper drawing shows a polyamide depth electrode with six platinum contacts and a special inner stylet that can be firmly attached to the pointer probe of the navigation system. The lower drawing shows the eight platinum/iridium microwires. Tips of microwires extend 1.5 to 5 mm beyond the tip of the depth electrode. (B) Low- and high-magnification photographs of electrodes. The upper panel shows the depth electrode with inserted microwires. The special inner stylet is also shown adjacent to the depth electrode. The length of the stylet shaft was equal to that of the depth electrode. The lower panel shows the tip of the wire electrode composed of eight microwires. Scale bars indicate 5 mm. (C) High-magnification view of the depth electrode with silicone fringe. Each silicone fringe was cut into a suitable shape and size. (D) Macroscopic view of the operative field after implantation of all the electrodes except microwires. Black arrowheads indicate depth electrodes inserted to hippocampus. White arrowhead denotes a trapezoid electrode locating the surface of parahippocampal gyrus. Asterisks show grid electrodes implanted to the lateral surface (black) and ventral temporal surface (white). The green dotted line represents the sylvian fissure.

Figure 2. Location of implanted electrodes in a patient with temporal lobe epilepsy. (A) Three-dimensional view of all the electrodes reconstructed from postoperative high-resolution computerized tomography. Asterisks indicate microwire-combined depth electrodes. R, right. (B) Three-dimensionally rendered MRI figures showing the location of microwire-combined depth electrodes in co-registered high-resolution computerized tomography. Axial and

coronal views of the electrodes targeted to the hippocampal head (top) and the subiculum (bottom). Yellow lines indicate the positions of the coronal sections shown in the right panel. Green dots denote the contacts of depth electrodes. (C) Left:axial view of planned and inserted trajectories. Green dotted lines show actually inserted electrodes while white lines represent planned trajectories. Right:high-magnification view measuring the gap between the target point and implanted point.

Figure 3. Spatial errors between the target point and implanted point. Each panel represents a three-dimensional display (upper left), Y-Z axis (upper right), X-Z axis (lower left) and X-Y axis (lower right), respectively. Center cross indicates target; circles show the actual position of the implanted electrodes.

Figure 4. Temporal stability of successful recording rate. 11-15 days after surgery showed the highest performance (mean: 13.6%) and 6-10 days showed the lowest (mean: 8.2%), respectively. No significant difference was observed among each recording period ($P = 0.65$; Kruskal-Wallis test). Bars show the standard deviations.

Figure 5. Comparison among single-unit firing rate (top), LFP (2^{nd} row), raw iEEG (3^{rd} row) and power spectrogram calculated from iEEG (bottom). X-axis represents time from clinical seizure onset. Spikes and LFP were recorded with the microwire placed in the right hippocampal head, and iEEG was recorded from the nearest electrode that covered the medial parahippocampalgyrus. Red dashed line represents clinical seizure onset. ERSP: event-related spectral perturbation.

Figure 6. Peristimulus-timehistograms of hippocampal neuron activityof a patient in response to visual presentation of photographs of close family members. 1^{st} column representthe firing rate for visual stimuli of family 1. 2^{nd}, 3^{rd} and 4^{th} column indicate the responses to the photographs of family 2, 3 and 4, respectively. X-axis represents time from visual stimulus onset, and Y-axis represents summated firing rate of 38 trials within the temporal 100-ms time bin. Dashed vertical lines indicate the onset and offset of visual stimulation (1-sec. presentation). Dashed horizontal lines in red indicate mean + 2 SD level of the spontaneous firing rate.

Table 1. Summary of patient characteristics

Subject	Age/sex	Num. of depth electrode (grid/strip electrode)	Laterality	Location	MRI findings	Successful recording
1	22 / F	2 (204)	L	H / S	L. hippocampal sclerosis	1/8
2	24 / M	4 (236)	L	H / S	L. cortical dysplasia	3/16
3	30 / M	2 (196)	L	H / Trigonum	L. periventricular nodular heterotopia	0 / 16
4	41 / F	4 (248)	B	H / S	Non-lesional	1/32
5	23 / M	2 (83)	L	Parietal	Non-lesional	1/ 16
6	37 / M	4 (198)	B	H / S	L. hippocampal sclerosis	6/32
7	35 / F	4 (210)	B	H / S	Non-lesional	0 /32
8	38 / F	4 (242)	B	H / S	Non-lesional	13 /32
9	15 / M	4 (158)	B	H / S	R. temporal cystic tumor	6 /32

Table 1. Summary of electrode number/location, MRI findings and clinical data. Subject 7 was excluded from data analysis because of damage to the ground/reference wire.L, left; R, right; B, bilateral; H, hippocampus; S, subiculum.

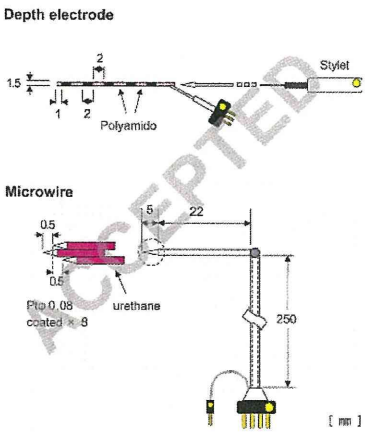
Depth electrode
2
1.5
Stylet
1
2
Polyamido
Microwire
0.5
5
22
0.5
Pt-Ir 0.08
coated × 8
urethane
250
[mm]

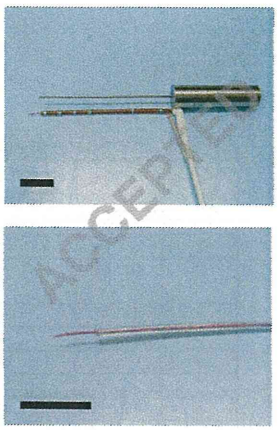

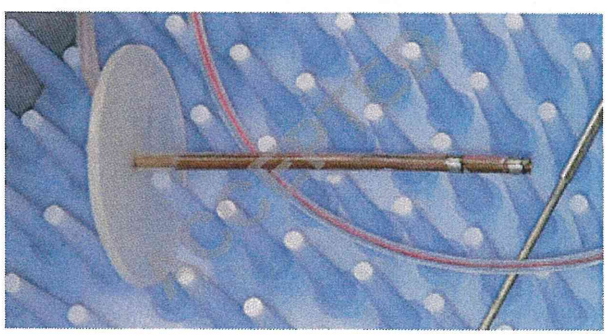

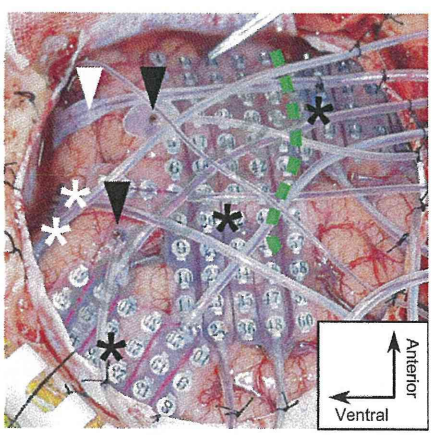
Anterior
Ventral

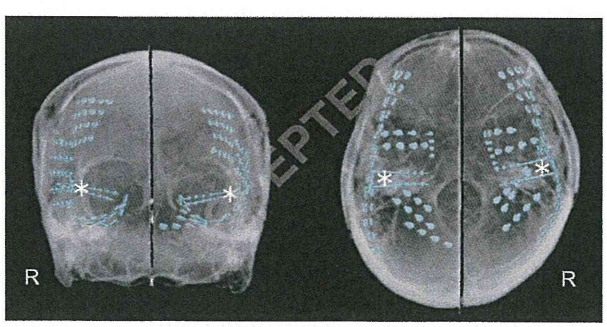
R
R

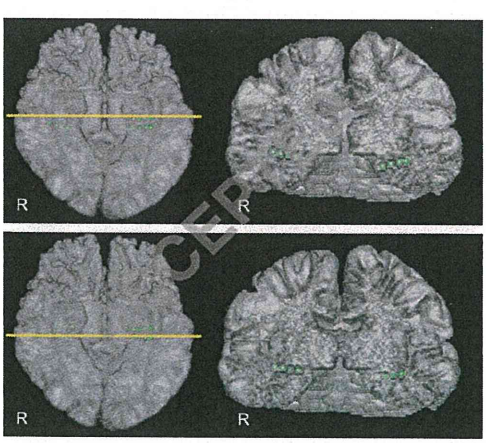
R
R
R
R

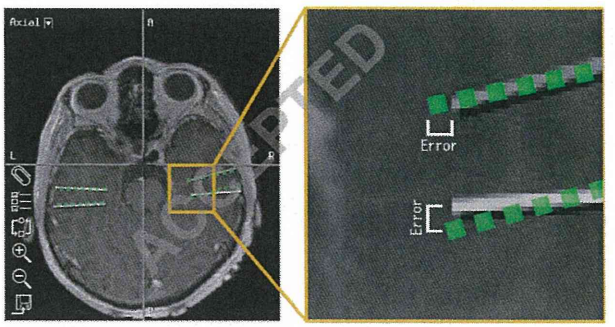
Axial
Error
Error

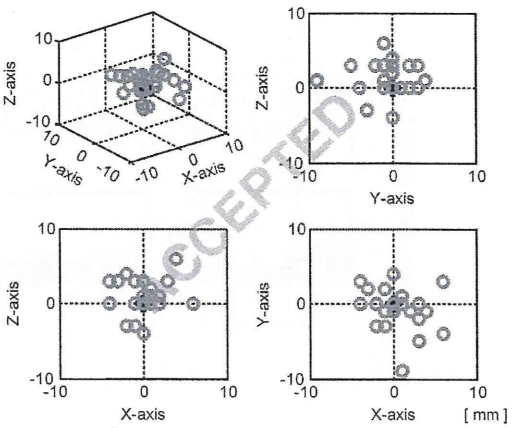
Z-axis
Y-axis
X-axis
Z-axis
Y-axis
Z-axis
X-axis
Y-axis
X-axis
[mm]

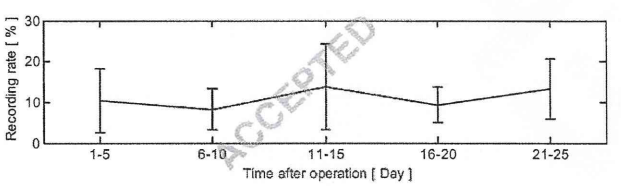
Recording rate [%]
1-5
6-10
11-15
16-20
21-25
Time after operation [Day]

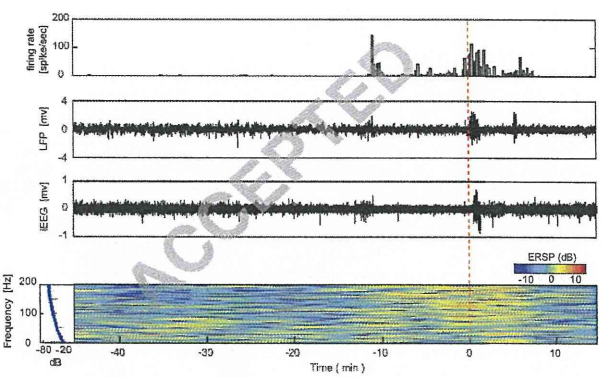
firing rate [sp/ks/sec]
LFP [mv]
IEEG [mv]
ERSP (dB)
Frequency [Hz]
dB
Time (min)

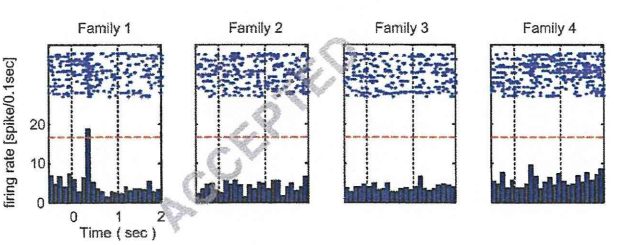
Family 1
Family 2
Family 3
Family 4
firing rate [spike/0.1sec]
Time (sec)

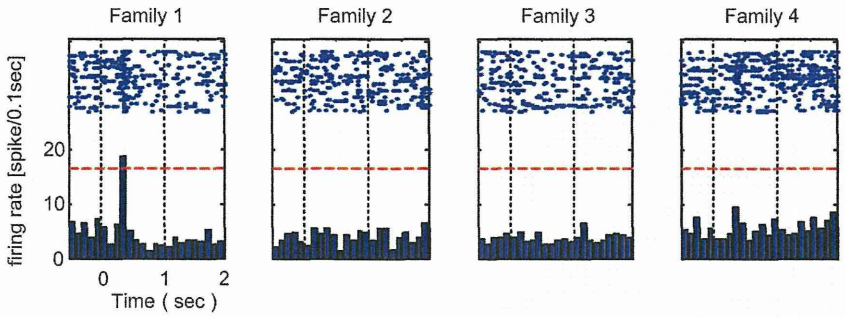

ARTICLE IN PRESS

Brain Stimulation xxx (2012) 1–9

Contents lists available at SciVerse ScienceDirect

Brain Stimulation

journal homepage: www.brainstimjrnl.com

Original Research

Scalp-recorded evoked potentials as a marker for afferent nerve impulse in clinical vagus nerve stimulation

Kenichi Usami [a], Kensuke Kawai [a,*], Masahiro Sonoo [b], Nobuhito Saito [a]

[a] Department of Neurosurgery, Graduate School of Medicine, The University of Tokyo, 7-3-1 Hongo, Bunkyo-ku, Tokyo 113-8655, Japan
[b] Department of Neurology, Teikyo University School of Medicine, Tokyo, Japan

ARTICLE INFO

Article history:
Received 27 April 2012
Received in revised form
19 August 2012
Accepted 18 September 2012
Available online xxx

Keywords:
Epilepsy
Evoked potential
Vagus nerve
Vagus nerve stimulation

ABSTRACT

Background: Vagus nerve stimulation (VNS) is a palliative treatment for drug resistant epilepsy for which the efficacy and safety are well established. Accumulating evidence suggests that ascending vagal signals modulate abnormal cortical excitability via various pathways. However, there is no direct evidence for an ascending conduction of neural impulses in a clinical case of VNS.
Objective: We recorded and analyzed the short-latency components of the vagus nerve (VN) evoked potential (EP) from the viewpoint of determining whether or not it is a marker for the ascending neural conduction.
Methods: EPs within 20 ms were prospectively recorded simultaneously from a surgical wound in the neck and at multiple scalp sites during implantation surgery in 25 patients with drug-resistant epilepsy. Electrical stimulation was delivered using the clinical VNS Therapy system. A recording was made before and after a muscle relaxant was administered, when changing the rostrocaudal position of stimulation, or when stimulating the ansa cervicalis instead of the VN.
Results: The short-latency components consisted of four peaks. The early component around 3 ms, which was most prominent in A1–Cz, remained unchanged after muscle relaxation while the later peaks disappeared. Rostral transition of the stimulation resulted in an earlier shift of the early component. The estimated conduction velocity was 27.4 ± 10.2 m/s. Stimulation of the ansa cervicalis induced no EP.
Conclusions: The early component was regarded as directly resulting from ascending neural conduction of A fibers of the VN, probably originating around the jugular foramen. Recording of VN-EP might document the cause of treatment failure in some patients.

Introduction

Vagus nerve stimulation (VNS) is a widely used adjunctive therapy for drug-resistant epilepsy [1]. Generally VNS reduces the frequency of seizure by approximately 50% in 50% of patients, which shows improvement over time. Independent of its anti-epileptic effects, its antidepressive effects and contribution to cognitive improvement have been suggested as well [2,3]. In contrast to its clinical usefulness and popularity, the underlying mechanisms of action in VNS have not been fully elucidated. In an animal model, VNS induced the expression of c-fos protein in vagus nuclei, the locus coeruleus, cochlear nuclei, the amygdala, the cingulate gyrus, and the retrosplenial cortex, indicating transsynaptic activation of the ascending pathways in the brain [4]. An increase in GABA transmission or a decrease in glutamate transmission in the mediocaudal nucleus of the solitary tract resulted in a reduction of susceptibility to limbic motor seizures [5]. Ascending modulation works on cortical excitability via various ascending pathways including the monoaminergic system [6–8]. Finally, in the cerebral cortex, which is directly associated with epileptogenicity, slow hyperpolarization of pyramidal neurons was induced by VNS [9].

In humans, an enhancement of local inhibition in the primary motor cortex and changes to cerebral blood flow in the thalamus and various regions of cerebral cortices have been observed in association with VNS [10,11]. However, there is no direct evidence

Conflicts of interest: Drs. Usami, Sonoo and Saito report no potential conflicts of interest. Dr. Kawai reports having received lecture fees from Nihon Kohden Corporation.

This work was supported partly by the Ministry of Health, Labour and Welfare of Japan (Grant for Comprehensive Research on Disability, Health and Welfare; H23-Nervous and Muscular-General-003) and partly by Grants-in-Aid for Scientific Research (A) 23240065 and (B) 21390405.

* Corresponding author. Tel.: +81 3 5800 8853; fax: +81 3 5800 8655.
E-mail address: kenkawai-tky@umin.net (K. Kawai).

1935-861X/$ – see front matter © 2012 Elsevier Inc. All rights reserved.
http://dx.doi.org/10.1016/j.brs.2012.09.007

Table 1
Characteristics of patients.

Pt. no.	Sex	Age at seizure onset	Age at start of VNS (yrs)	Diagnosis	Type of seizure	Follow-up duration (month)	Seizure reduction at last follow-up[b] (%)	Antiepileptic drugs
1	M	27 y	30	TLE, postencephalitis	CPS	19	<50	CBZ, PHT, GBP, PHT, LTG
2	M	1 y	13	LGS	GTS, AA, DA	19	<50	VPA, PB, CLB, LTG
3	F	9 m	15	SGE, post West synd.	GTS	19	0	VPA, LTG
4	M	34 y	40	TLE, postencephalitis	CPS, SGTCS	16	>70	PHT, GBP, CLB, VPA, CZP, CLB
5	F	8 m	12	SGE, tuberous sclerosis	CPS	16	<50	VPA, LTG
6	M	23 y	47	TLE	CPS, SGTCS	16	>70	VPA, PHT, CBZ
7	M	2 y	9	FLE, cortical dysplasia	CPS, GTS	16	>70	VPA, CLB, ZNS
8	M	10 y	25	TLE, postencephalitis	CPS, SGTCS	15	<50	LEV, CLB
9	M	25 y	28	TLE, postencephalitis	CPS, SGTCS	13	>50	VPA, PHT, PB, LTG, TPM
10	F	9 m	9	SGE, tuberous sclerosis	SPS, CPS, AA	12	<50	CBZ, TPM, LTG, LEV
11	F	9 y	15	TLE	SPS, CPS, GCS	12	<50	LTG
12	M	7 m	3	SGE, post West synd.	GTS, AA, MS	11	>50	VPA, CZP, ZNS, LTG
13	F	3 y	14	LGS	GTS	11	0	VPA
14	F	31 y	36	FLE	SPS	11	<50	VPA, CBZ, TPM
15	M	1 y	3	CGE	GTS, AA, DA	0[a]	0	PB, ZNS, CZP, LEV
16	M	11 y	13	TLE, postencephalitis	CPS, SGTCS	11	<50	CLB, TPM, LTG
17	M	11 y	32	TLE	SPS, CPS	10	<50	VPA, CBZ, PHT
18	M	3 y	9	TLE	CPS	10	<50	CBZ, CLB, LTG, TPM
19	F	1 y	29	FLE, TLE	CPS, SGTS	9	>50	CBZ, LTG, LEV
20	F	6 y	27	FLE, TLE, HH	CPS, SGTS	9	<50	VPA, CBZ, ZNS, LEV
21	M	15 y	39	TLE	SPS, CPS	9	<50	VPA, PHT, ZNS, CLB, CZP
22	F	12 y	22	FLE, TLE	SPS, CPS	6	>70	PHT, CZP, LTG
23	M	7 y	12	TLE	CPS, SGCS	3	>50	LTG, LEV
24	F	1 y	28	LGS, tuberous sclerosis	GTS	3	<50	CBZ, PHT, LTG
25	M	6 y	18	FLE	GTS	2	>50	VPA, PHT, ZNS, CLB

TLE: temporal lobe epilepsy, LGS: Lennox-Gastaut syndrome, SGE: symptomatic generalized epilepsy, FLE: frontal lobe epilepsy, CGE: cryptogenic generalized epilepsy, HH: hypothalamic hamartoma, CPS: complex partial seizure, GTS: generalized tonic seizure, AA: atypical absence, DA: drop attack, SGTCS: secondary generalized tonic clonic seizure, SPS: simple partial seizure, GCS: generalized clonic seizure, MS: myoclonic seizure, SGTS: secondary generalized tonic seizure, SGCS: secondary generalized clonic seizure, CBZ: carbamazepine, GBP: gabapentine, CLB: clobazam, PHT: phenytoin, LTG: lamotrigine, VPA: valproate, PB: phenobarbital, CZP: clonazepam, ZNS: zonisamide, LEV: levetiracetam, TPM: topiramate.
[a] VNS therapy system was removed 3 weeks after implant surgery due to infection in Patient #15.
[b] Seizure reduction is expressed as % reduction of preoperative frequency.

that ascending conduction of neural impulses is indeed generated by an electrical stimulation of the cervical vagus nerve (VN). Hammond et al. first recorded scalp potentials evoked by clinical VNS [12]. While they observed a large negative peak at around 12 ms following stimulation, it disappeared after administration of a muscle relaxant, indicating that it was an electromyogram of the pharyngeal muscles induced by descending impulses. Tougas et al. described scalp potentials with three peaks of latencies as long as 71 ms, 194 ms and 328 ms [13]. Considering such long latencies, the potentials they observed were regarded as responses induced by polysynaptic neural transmission, not directly reflecting ascending conduction of the VN.

To examine our hypothesis that, in a clinical setting, stimulation of the VN should generate recordable evoked potentials (EPs), such as the early peaks of somatosensory EP and auditory brainstem responses, we prospectively recorded and analyzed the short-latency components of VN-EPs in humans from the viewpoint of whether or not it is a direct marker for the ascending neural conduction.

Materials and methods

Subjects

The subjects of this study were 25 consecutive patients who underwent implantation of the VNS Therapy system (Cyberonics, Houston, TX, USA) for the treatment of drug-resistant epilepsy (Table 1). Board-certified epileptologists made diagnoses of drug-resistant epilepsy and determined an indication for VNS therapy through a routine presurgical evaluation, including long-term video EEG, MRI, ECD-SPECT, IMZ-SPECT, FDG-PET, and neuropsychological assessment. Fifteen of the patients were male and 10 were female. Age distributions were 3–47, median 18 years old. Eleven of them had preceding craniotomy for epilepsy surgery. The number of antiepileptic drugs being administered to those patients at the time of study were 1–6, median 3.0. General and neurological examinations confirmed that none of the patients had systemic and neurological diseases other than epilepsy.

This study was approved by the local ethics committee (The University of Tokyo, Faculty of Medicine; approval number 2592; date of approval June 22, 2009). Written informed consent for this study was obtained from the patients and/or their families.

Recording of VN-EP during VNS implantation

Vagus nerve EP was recorded during implantation surgery of the VNS Therapy system under general anesthesia. The agents used for induction of anesthesia were sodium thiopental in 14 patients, with a mean dosage of 5.1 mg/kg; propofol in 10 patients, with a mean dosage of 2.2 mg/kg; and nitrous oxide in one patient. Muscle relaxants used at the time of anesthetic induction were vecuronium bromide in 22 patients and rocuronium bromide in 3 patients. In all patients, the time between the induction of anesthesia and the start of VN-EP recording was 60–90 min. General anesthesia was maintained with sevoflurane in all patients. Needle electrodes were placed in the patients' scalps at A1, A2, C3, C4, Cz and T5, according to the international 10–20 system. These were connected to a signal processor input box (Neuropack MEB-2200, Nihon Kohden Corporation, Tokyo, Japan). Additionally we placed an A1a electrode on the left

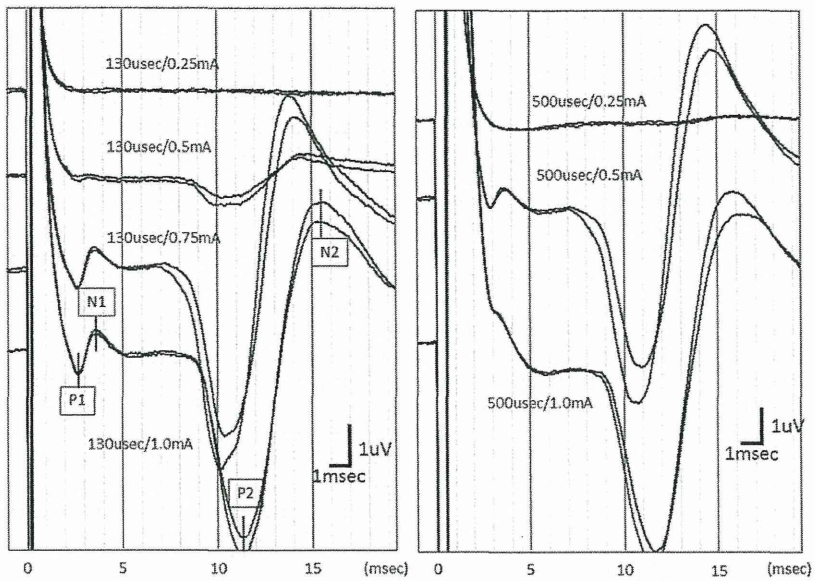

Figure 1. Representative waveforms evoked by various parameters of vagus nerve stimulation. The evoked potentials during 20 ms, beginning 1 ms before each pulse of the VNS, were recorded from scalp electrodes A1–Cz with 50-Hz high-pass, 3000-Hz low-pass, and 50-Hz notch filters, and were averaged for 1000 stimuli. Two representative traces of A1–Cz from a patient are presented. A current of 0.25 mA did not evoke any discernable potential, irrespective of pulse width. As the current and pulse width were increased, small biphasic peaks around 3 ms (P1, N1) immediately following a large stimulation artifact, and large biphasic peaks (P2, N2) around 10 ms, appeared. Further increase in the current and pulse width resulted in an increase of N1 amplitude, but the P1–N1 complex evoked by 500 μs and 1.0 mA was buried in the downslope of the initial stimulation wave and could be recognized only as a tiny notch and a shoulder.

mastoid process and an A1b electrode on the midpoint of A1a and T5. A gelatinous tape electrode (Disposable Earth Electrode, GE Health Care, Tokyo, Japan) was attached circumferentially at the level of the jaw and nape and was connected to the ground to reduce the artifact of stimulation. In 5 patients, an endotracheal tube with electrodes was used for recording of the laryngopharyngeal electromyogram. The tube was equipped with two pairs of bipolar electrodes on each side approximately 4 cm rostral from the tip.

A skin incision was made in the anterior neck approximately 3 cm above the left clavicle. A 3-cm length of the left VN was exposed and completely isolated from the surrounding tissue. The helical electrodes of the VNS Therapy system were coiled around the nerve and connected to the programmable pulse generator. The anchor tether was left unplaced so that we could move the electrodes rostrocaudally along the nerve. After we confirmed with a test-stimulation that there was no adverse event and that the impedance of the electrode was within the expected range, we started stimulation with the VNS Therapy system. We used the magnet mode for stimulation and the parameters were as follows: frequency, 30 Hz; pulse width, 130–750 μs; current, 0.25–2.00 mA; on-time, 60 s. Then we subdermally inserted two needle electrodes to the medial and lateral walls of the surgical wound and connected them to the external trigger of the signal processor.

The montages used for recording were A1–Cz, A2–Cz, C3–Cz, C4–Cz, T5–Cz, A1a–Cz, and A1b–Cz, where Cz was used as a common reference. The signals were amplified and digitized with a sampling rate of 30,000 Hz. The EPs for 20 ms, starting at 1 ms before the external trigger, were recorded with 50-Hz high-pass, 3000-Hz low-pass, and 50-Hz notch filters and were averaged for 1000 recordings. Averaging was started several seconds after the start of stimulation in order to avoid a 2-s ramp-up period, and continued for approximately 33 s (1000 stimuli). The external signal from the needle electrodes close to the VNS helical electrodes in the surgical wound was used as a trigger for averaging.

We recorded the potential at least three times for each condition and for each position of the electrodes. We started each recording several seconds after we turned on the VNS stimulation by placing a magnet over the pulse generator.

In 13 patients, EPs were recorded both before and after the administration of a muscle relaxant. In 3 patients, recording was done without a muscle relaxant. In the remaining 9 patients, recording was done only after a muscle relaxant had been administered. The recording was started 80–100 min after induction of general anesthesia. After we finished the recording of the above-mentioned 13 patients without muscle relaxants, 0.04 mg/kg vecuronium bromide was administered intravenously. After waiting for 2 min, recording of the same patients under muscle relaxation was started.

In some patients, we added the following recordings: First, the helical electrodes of the VNS Therapy system were coiled around the ansa cervicalis and the potentials were recorded before routine recording with stimulation of the VN, for the purpose of investigating whether the potentials were specific for stimulation of the VN ($N = 5$). During surgery, the ansa cervicalis appears over the jugular vein and carotid sheath as we dissect the cervical tissues. Its diameter is thinner than the VN and varies markedly among patients, but it is identifiable in all patients under an operative microscope. Second, the helical electrodes were moved rostrocaudally and measurements were performed at each position, for the purpose of determining whether the conduction is ascending or descending, and to calculate the estimated value of conduction velocity of the VN ($N = 14$). The nerve conduction velocity (NCV) was calculated as follows:

$$NCV = \Delta/(Lc - Lr),$$

where Δ is the distance between the caudal stimulation point and the rostral stimulation point, and Lc and Lr are latencies of the peak of N1 measured at the caudal and rostral stimulation points, respectively. The distance of movement of the helical electrode was visually determined using a tape measure under a surgical microscope (Supplement 1). Furthermore, additional recordings were done while moving the trigger electrodes from within the wound to 5 cm outside of the wound, changing the distance between the trigger electrodes and the helical electrodes of VNS, for the purpose of confirming the stability and reliability of the trigger electrodes ($N = 1$).

The total recording time was less than 1 h in all patients. After all measurements had been completed, we placed the pulse generator in a subcutaneous pocket of the left anterior chest and closed the wound. There were no adverse events associated with this study.

Data analysis

The EPs were saved as image data of acquired traces and as numerical data with a timeline in all patients. Two traces out of three were selected from the viewpoint of stability and consistency by visually inspecting the traces.

First, we determined the latency of peaks in waveforms using a cursor of the signal processor by visual inspection. The processor began timing from zero at the moment of the external trigger. An average value of the two traces was used. In those patients in whom more than one recording was done due to changing the position of stimulation, we used an averaged value of those recordings to present the rough latency of the P1–N1 complex, because the final electrode position at the end of implantation surgery was approximately at the midpoint of two stimulation positions.

In some patients, early peaks were buried in the downslope of the initial stimulation wave and were identified only as a tiny notch and a shoulder, so it was difficult to exactly determine the latency of the peaks (see Fig. 1). Therefore, secondly, we determined their latencies in the estimated waveform after elimination of the initial stimulation wave. Curve fitting to an exponential function was applied to the range between 0.8–1.8 ms of the original numerical data using Microsoft Excel. Then we extracted the evoked component by subtracting the approximated value from the original value at each time point (Supplement 2):

$$Pi = Oi - \exp(Ti),$$

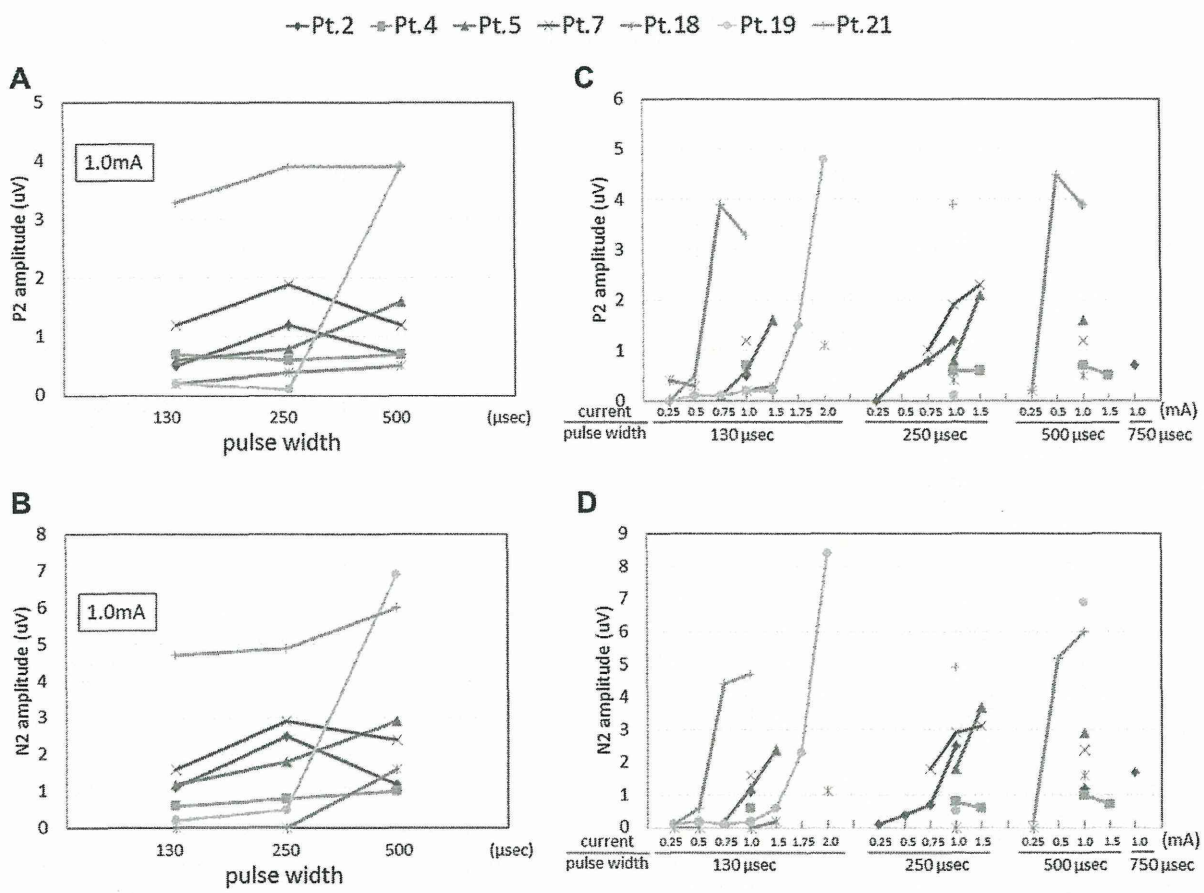

Figure 2. Association between the P2 and N2 amplitudes and the VNS parameters in each patient ($n = 7$). Each line represents a patient. (A) and (B) demonstrate the amplitudes of P2 and N2, respectively, when stimulated with three pulse widths at a fixed current of 1.0 mA. The pulse width did not seem to significantly affect the amplitudes of P2 and N2 in all patients except one (Patient # 19). (C) and (D) demonstrate the amplitudes of P2 and N2, respectively, when stimulated with various currents. The current seemed to affect the amplitudes in a sigmoid fashion.

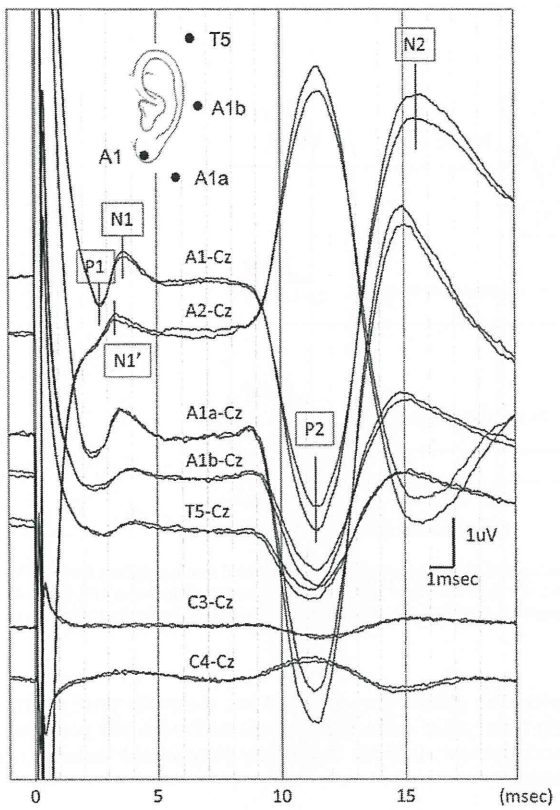

Figure 3. Vagus nerve evoked potentials recorded in different montages. Two traces from a single patient without muscle relaxation. The parameters of VNS were a current of 1.0 mA, a pulse width of 130 μs, and a frequency of 30 Hz. The early negative peak (N1) was most prominent in montages A1–Cz and A1a–Cz. It gradually decreased its amplitude as the exploring electrodes separated away from the skullbase from A1a to A1b to T5. A smaller negative peak (N1′) was noted in A2–Cz slightly earlier than the N1 observed in A1–Cz. Large peaks (P2, N2) of the late component showed a phase reversal between the sides of exploring electrodes.

where *Pi* is the estimated evoked component at time point *i*, *Oi* is the original value of potential at time point *i*, and *Ti* is the time at *i*. Using the thus extracted data, we determined the latency and amplitude of early peaks. The signal processor saved the original data, starting 1 ms before the trigger point. Time zero was defined as the time point where a huge (>1 μV) abrupt change of amplitude occurred for around 1 ms. The baseline amplitude was defined as the mean amplitude of the first 1 ms. The amplitude of the early component was defined as the difference between the amplitudes of positive and negative peaks. The appropriateness of approximation with an exponential function was confirmed in the data where no early components were evoked, i.e., stimulation of the ansa cervicalis and stimulation with minimal parameters, that is, 0.25 mA and 130 μs.

To assess the effect of stimulation parameters on the amplitudes of the early and late components, we drew input–output curves. The amplitude of P2 and N2 were determined as the absolute difference from baseline. Determination of the amplitude of the P1–N1 complex has been described above. In 4 patients (#16, #17, #18, #19), whose recordings were done with caudal and rostral stimulations, measurements with various parameters were done only during caudal stimulation.

The values were presented as mean ± standard deviation among patients.

Results

Waveform of VN-EP

The waveforms evoked by clinical VNS were highly reproducible within each patient and consistent among the patients. The initial stimulation wave was a huge wave consisting of a momentary biphasic spike and a subsequent exponential downslope in all patients. Following the initial stimulation wave, we typically observed four peaks in the waveform (Fig. 1). The early and late peaks were with a latency shorter and longer than 5 ms, respectively. We named the early smaller positive and negative peaks as P1 and N1, respectively, and the subsequent larger positive and negative peaks as P2 and N2, respectively.

The P1–N1 complex was recognizable in all patients except two, in whom no waveform was observed in one (Patient #20) and only a late component in the other (Patient #3). In Patient #20, various parameters of stimulation were applied but no potentials other than the initial stimulation wave were generated. In Patient #3, a pulse width of only 500 μs was used. In patients in whom visual determination of N1 was possible ($N = 23$), its latency in A1–Cz was 3.3 ± 0.4 ms (range 2.5–4.2).

The P2–N2 complex consisted of a large positive peak (P2) at 6.4–11.1 ms and a subsequent large negative peak (N2) at 9.2–15.1 ms when the exploring electrode was on the left side. The P2–N2 complex was identified in all patients in whom recording was done without muscle relaxants except two, in whom no waveform was observed in one (#20) and only an early component in the other (#17).

Effect of stimulation parameters

Minimal stimulation of the VN with 0.25 mA and 130 μs did not induce the early and late complexes but did reproducibly induce the initial stimulation wave (Fig. 1). When the pulse width and/or current were increased, it seemed that the amplitude of the P1–N1 complex increased but the latency did not. The downslope of the initial stimulation wave was prolonged as well. A further increase to 500 μs and 1.0 mA resulted in a paradoxical decrease of the P1–N1 complex, so that it was only identifiable as a tiny notch and a shoulder in the downslope. Therefore, the amplitude of the P1–N1 complex, as determined by visual inspection, did not reflect the genuine amplitude of the EP. We measured the P1–N1 amplitude in the estimated waveform after elimination of the initial stimulation wave, which is presented below.

The association between the P2 and N2 amplitudes and the VNS parameters in each patient is presented in Fig. 2. The pulse width did not seem to significantly affect the amplitudes of P2 and N2, whereas the current did seem to affect their amplitudes in a sigmoid fashion.

Topographical distribution of EP

The P1–N1 and P2–N2 complexes were most prominent in montages A1–Cz and A1a–Cz (Fig. 3). They gradually decreased as the exploring electrodes separated away from the skullbase, from A1a to A1b to T5. In A2–Cz, the phase of the initial stimulation wave and the P2–N2 complex were reversed, but the phase of the early complex (N1′) was not reversed. The latency of the N1′ peak in A2–Cz was slightly earlier than the N1 peak in A1–Cz. The waveform of the P2–N2 complex was not only reversed but almost completely symmetrical in A1–Cz and A2–Cz. The P2–N2 complex was discernable in C3–Cz and C4–Cz as a smaller similarity of

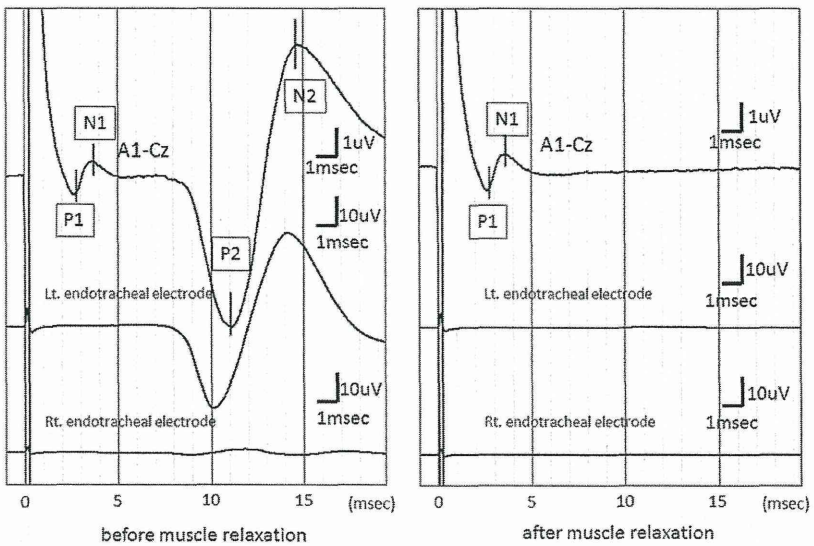

Figure 4. Vagus nerve evoked potential, endotracheal electromyogram (EMG), and effect of muscle relaxation. The endotracheal EMG was recorded dominantly from the left side. Its waveform was a much larger and slightly earlier similarity of the late components in A1–Cz. Note the scale is different between the top trace and the lower two traces. After administration of a muscle relaxant, the endotracheal EMG and the late component in A1–Cz disappeared, while the early component was unchanged. Representative traces from a patient are presented.

A1–Cz and A2–Cz, respectively, but the P1–N1 complex was not discernable in C3–Cz and C4–Cz.

Effect of muscle relaxation

Under muscle relaxation, the initial stimulation wave and the P1–N1 complex remained unchanged, while the P2–N2 complex completely disappeared (Fig. 4). The disappearance of the late components and preservation of the early component under muscle relaxation were observed in all of the 13 patients in whom both of the components were detected before muscle relaxation. Simultaneous recording from the endotracheal electrodes demonstrated no early component but rather a late component similar to the P2–N2 complex in A1–Cz. This was more prominent on the left side and its waveform was a much larger similarity of the P2–N2 complex. The phases were identical but the peaks were approximately 1 ms earlier in the endotracheal electrodes. The potential in the endotracheal electrode completely disappeared under muscle relaxation.

Stimulation of ansa cervicalis

Stimulation of the ansa cervicalis resulted in a consistent and reproducible stimulation wave, but no other discernable potentials were evoked including the P1–N1 and P2–N2 complexes (Fig. 5).

Effect of stimulating position

Evoked potentials were recorded while changing the rostrocaudal position of helical stimulation electrodes along the VN

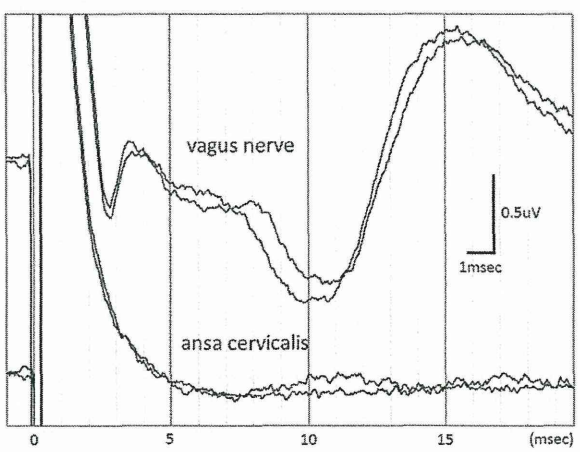

Figure 5. No potential was evoked when the ansa cervicalis was stimulated. Representative traces are presented from a single patient. Stimulation parameters were a current of 1.0 mA, a frequency of 30 Hz, and a pulse width of 130 μs.

Table 2
Distance of electrode movement, visually determined latency of N1, and estimated value of nerve conduction velocity.

Patient #	Δ (mm)	Lc (ms)	Lr (ms)	Lr-Lc (ms)	NCV (m/s)
8	12	3.1	3.5	−0.3	N/A
9	12	3.7	3.1	0.6	19.4
10	8	3.6	3.3	0.3	25.8
11	6	3.2	3.6	−0.3	N/A
12	5	3.0	2.3	0.7	6.8
14	11	3.0	2.7	0.3	32.4
16	10	4.0	3.8	0.2	41.7
17	7.5	3.6	3.4	0.2	37.5
18	9	2.9	2.6	0.3	30.0
19	14	2.7	2.2	0.5	28.0
22	10	3.0	2.6	0.4	25.0
23	12	3.1	V/U		N/A
24	8	2.9	3.2	−0.3	N/A
25	9	3.7	V/U		N/A
Mean	9.5	3.3	3.0	0.4	27.4
SD	2.5	0.4	0.5	0.2	10.2

Δ, distance (mm) of transition from the caudal stimulating point to the rostral stimulating point. Lc (ms), latency of N1 measured with caudal stimulation. Lr (ms), latency of N1 measured with rostral stimulation. NCV (m/s), nerve conduction velocity, calculated as Δ/(Lc−Lr). V/U, visually undetermined. SD, standard deviation.

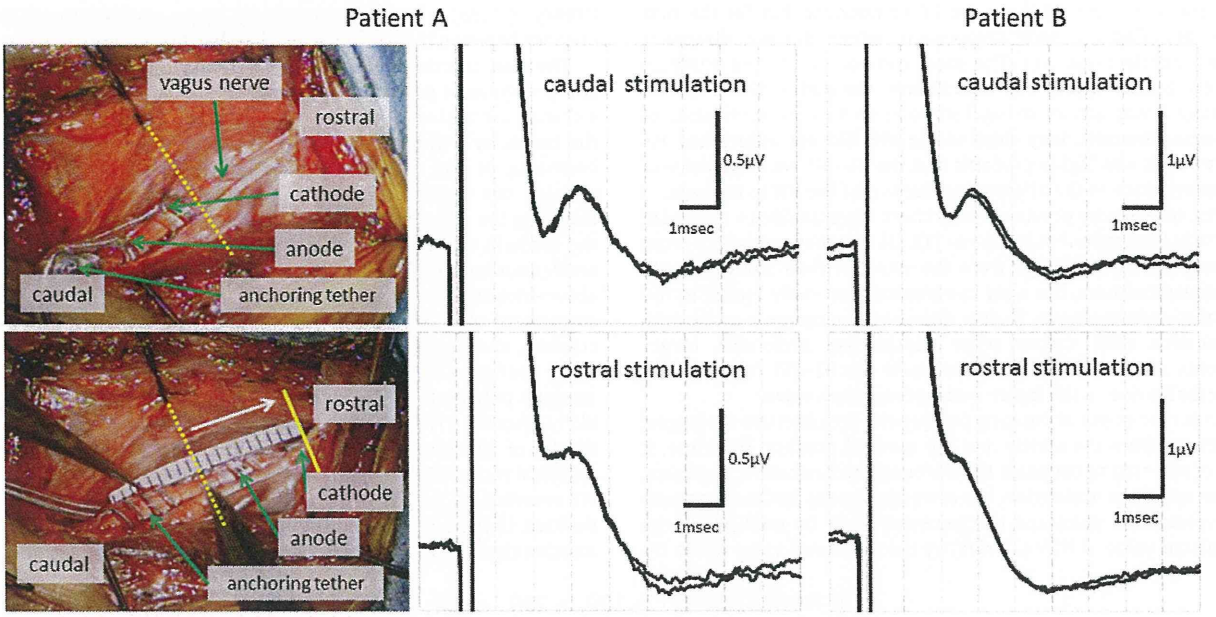

Figure 6. Effect of stimulation position. Evoked potentials were recorded while changing the rostrocaudal position of the helical stimulation electrode along the vagus nerve. In this patient (Patient #14 in Table 1), the rostral end of the cathode was moved from the yellow dotted line to the yellow solid line. The movement was 11 mm. Representative recordings in 2 patients are presented. In Patient A (Patient #14 in Table 1), an earlier shift of the P1–N1 complex by rostral transition of stimulation is clearly discernable. In Patient B (Patient #23 in Table 1), the earlier shift is not very clear.

in 14 patients. The distance of movement was 9.5 ± 2.5 mm (Table 2). With the rostral movement of the stimulation electrodes, an earlier shift of the P1–N1 complex was observed by visual inspection in 11 patients (Fig. 6). In the remaining 3 patients, there was no recognizable latency shift by visual inspection. In 9 patients in whom N1 latencies in both rostral and caudal stimulation could be determined by visual inspection, the estimated nerve conduction velocity was 27.4 ± 10.2 m/s (Table 2).

Extraction of P1–N1 complex and estimation of nerve conduction velocity

An exponential curve estimated from the initial 0.8–1.8 ms was well fit to the subsequent 1.8–5.0 ms of the original data where the ansa cervicalis was stimulated ($N = 5$, correlation coefficient 0.967) and the stimulation parameters were minimal ($N = 4$, correlation coefficient 0.942). We regarded the approximation method as acceptable and used it as another determination method of P1–N1 complex latencies and amplitude, instead of visual determination.

Using this approximation and extraction of the waveform, the P1–N1 complex became clearer so that the peaks could be determined ($N = 14$). Table 3 is a summary of the latencies thus determined in all patients. The latencies of P1 and N1 were 2.5 ± 0.3 ms and 3.6 ± 0.5 ms, respectively, which were consistent with the values determined by visual inspection in 11 patients. The estimated nerve conduction velocity, calculated from a shift of N1 latency and the distance of stimulation points, was 30.4 ± 15.4 m/s. Fig. 7 demonstrates the association of the P1–N1 complex amplitude with stimulation parameters. In 7 of 9 patients, an increase in the stimulation current resulted in an associated increase in amplitude. The pulse width did not affect the amplitude.

Effect of position of trigger electrodes

Moving the trigger-electrode from within the surgical wound to 5 cm outside of the wound did not cause any changes in the waveform and latencies of the EP.

Discussion

A previous study by Hammond et al. demonstrated that the late component of VN-EP had been recorded in a clinical setting [12]. They suggested that the EP was a laryngopharyngeal electromyogram because it disappeared after the administration of a muscle

Table 3
Latencies of P1 and N1 determined by curve fitting, and estimated nerve conduction velocity.

Patient #	Δ (mm)	Latency of P1 (ms)			Latency of N1 (ms)			NCV (m/s)
		Distal	Proximal	Mean	Distal	Proximal	Mean	
8	12	2.6	3.1	2.9	3.8	4.2	4.0	N/A
9	12	2.9	2.5	2.7	4.1	3.5	3.8	21.6
10	8	2.6	2.5	2.6	3.9	3.7	3.8	28.1
11	6	2.5	2.4	2.5	4.0	3.8	3.9	37.5
12	5	2.4	1.8	2.1	3.7	3.0	3.4	7.6
14	11	2.4	2.2	2.3	3.6	3.3	3.4	31.0
16	10	3.1	2.9	3.0	4.6	4.6	4.6	N/A
17	7.5	2.9	2.7	2.8	4.0	3.8	3.9	26.8
18	9	2.3	2.2	2.3	3.1	2.7	2.9	25.4
19	14	2.5	1.9	2.2	3.3	2.8	3.1	34.1
22	10	2.5	2.3	2.4	3.6	3.2	3.4	23.8
23	12	2.4	2.0	2.2	3.4	3.1	3.2	33.3
24	8	2.2	2.1	2.2	3.2	3.1	3.2	72.7
25	9	2.8	2.7	2.7	3.8	3.5	3.7	23.1
Mean	9.5			2.5			3.6	30.4
SD	2.5			0.3			0.5	15.4

Δ, distance (mm) of transition from the caudal stimulating point to the rostral stimulating point. NCV (m/s), nerve conduction velocity, calculated from shift of N1 latency and Δ. SD, standard deviation.